10.1098/rspa.2001.0958

THE ROYAL SOCIETY

Sea waves and mass transport on a sloping beach

By Paolo Blondeaux, Maurizio Brocchini and Giovanna Vittori

Dipartimento di Ingegneria Ambientale, Università di Genova, Via Montallegro 1, 16145 Genova, Italy

Received 18 May 2001; accepted 14 December 2001; published online 5 July 2002

The steady streaming induced by a sea wave shoaling on a sloping beach and partly reflected at the coastline is determined in the region seaward of the breaker line. Shallow waters and waves of small amplitude are considered. Moreover, the Reynolds number is assumed to be large but still within the laminar regime and the flow domain is split into a bottom boundary layer and a core region. For an incoming wave which is fully absorbed at the coast the solution shows that close to the bottom the steady streaming is onshore directed even though the depth-averaged value represents an offshore directed flow. Moreover, the vertical velocity distribution depends on the ratio between the wave amplitude a^* and the thickness δ^* of the bottom boundary layer. For a fully reflected wave, steady recirculation cells are induced, the form and strength of which depend on the ratio a^*/δ^*. A complex flow is generated for reflection coefficients falling between 0 and 1.

Keywords: waves; steady streaming; undertow; sloping beach

1. Introduction

When approaching the coast, sea waves propagate on decreasing water depths, their profile steepens and they eventually break. Then the shore is reached and waves exhaust themselves in the form of thin sheets of water rushing up and down the beach face. Although the main water motion is to and fro, because of nonlinear effects the waves themselves induce a steady streaming and a net flux of water. For a discussion of the physical mechanism by which an oscillatory flow generates a steady streaming, the interested reader is referred to the recent review paper by Riley (2001). In the surf zone this steady drift can be very strong, since wave amplitudes attain large values and nonlinear effects are quite relevant. Offshore of the breaker line the steady-velocity components are often weak when compared with the fluctuating ones. Nevertheless, the former still play a significant role in many transport phenomena and, in particular, they have a strong influence on sediment transport because of their persistence. While steady currents induced by waves in the surf region have been studied by many researchers (see the contributions of Dally & Dean (1984), Svendsen (1984), Stive & Wind (1986), Svendsen *et al.* (1987), Deigaard *et al.* (1991), Stive & De Vriend (1994), Cox *et al.* (1995) and the references cited therein), much less is known about the structure of the steady streaming offshore of the breaker line. The existence of a steady drift associated with the propagation of a sea wave was first pointed out by Stokes (1847), who treated the problem by using the classical potential

wave theory. Then Longuet-Higgins (1953) tackled the problem of wave propagation and current generation in waters of constant depth with due consideration of fluid viscosity. For large Reynolds numbers, both surface and bottom boundary layers should be introduced.

Inside the bottom boundary layer, which has a thickness δ^* of order $\sqrt{2\nu^*/\omega^*}$ (ν^* being the kinematic viscosity of the fluid and ω^* the angular frequency of the surface gravity wave), the steady-velocity component is forced by the time-averaged Reynolds stresses resulting from the wave field (Phillips 1977; Craik 1982; Mei 1989). In particular, the steady-velocity component tends to a constant value at the edge of this bottom boundary layer. Near the surface, a thin boundary layer is present which is best studied by using curvilinear coordinates which fit the wavy surface. Within this layer, vorticity is much smaller than that present in the bottom boundary layer and has weaker effects on the mean mass transport.

The evaluation of the steady streaming outside the bottom and surface boundary layers deserves special attention. If attenuation of the wave amplitude in the direction of propagation is ignored, the induced streaming is strictly horizontal and independent of the horizontal coordinate. Hence, the vertical distribution of the velocity profile is provided by the 'creeping-flow approximation'. Indeed inertia terms identically vanish and the phenomenon is controlled by viscous diffusion. However, the wave amplitude a^* decays in the direction of wave propagation at a rate which is of order $a^*\delta^*/(L^*)^2$, L^* being the length of the wave. In this case, viscous terms are much larger than inertia terms only when $\delta^* \gg (a^*/L^*)a^*$. However, for field conditions δ^* is much smaller than $(a^*/L^*)a^*$ and viscous terms are negligible except within a second layer close to the bottom, the thickness of which turns out to be of order $L^*\sqrt{\delta^* L^*/(a^*)^2}$. The existence of a second thicker layer, in which convective inertia and viscous diffusion are equally important, was first pointed out by Stuart (1966) when analysing the oscillatory flow around a circular cylinder, while the phenomenon in the case of free-surface waves was investigated by Dore (1976) and Haddon & Riley (1983). These analyses as well as most of the subsequent investigations of the problem—until the recent and interesting investigations of Iskandarani & Liu (1991*a*, *b*) and Wen & Liu (1994)—have been carried out considering constant water depths. A further common assumption is that of wave propagation over an impermeable bottom even though studies exist of the phenomenon over a permeable bed (e.g. Liu 1977).

Quite often the seabed is covered with bed forms of different size. The steady-velocity components over a rippled bed have been investigated by many authors (Lyne 1971; Sleath 1976; Vittori 1989; Hara & Mei 1989; Blondeaux 1990), who, however, focused their attention on the velocity components which are spatially periodic with a wavelength equal to that of the ripples. In this case the existence of a second layer, in which convective inertia is as large as diffusion, was revealed by Hara & Mei (1989), who considered two asymptotic conditions. In the first case, weak fluid oscillations were considered, while in the second case ripples were assumed to be of small amplitude. The mechanism generating a steady streaming independent of the longitudinal coordinate was studied by Vittori & Blondeaux (1996), who, however, did not consider the flow far from the bottom boundary layer. The flow over bedforms characterized by wavelengths of the same order of magnitude of the length of sea waves and by large amplitudes was investigated by Riley (1984) with the aim of studying the interaction of sand waves and multiple bars (see, for example, Komar

(1998) for a description of these morphological patterns) with propagating waves. The same topic has been recently investigated by Yu & Mei (2000), who showed that periodic patterns of longshore bars are not generated by an instability mechanism but they are a forced phenomenon due to the non-uniformity of the wave amplitude envelope generated by a propagating wave which is partly reflected at the coast. Although the local slope differs from zero, because of the presence of the bedforms, the average water depth is constant and the analyses do not provide information on the steady streaming induced by waves which propagate over a sloping bottom.

A general formula to evaluate the steady streaming induced by nonlinear effects within the bottom boundary layer of a three-dimensional wave of small amplitude propagating over an arbitrary bottom profile was provided by Hunt & Johns (1963), who, however, did not consider the flow far from the bottom. Carter *et al*. (1973) applied these results to compute the velocity field at the bottom of a sea wave which approaches the coastline and is partly reflected at the beach. To evaluate the irrotational velocity components and, in particular, the beach reflectivity, Carter *et al*. (1973) used empirical data. The same problem, with the aim of investigating the mechanism leading to the appearance of a series of sand bars parallel to the shoreline was tackled by Lau & Travis (1973), who considered beaches characterized by very gentle constant slopes such that the wavefield could be locally described in terms of a linear Stokes wave over a constant depth. As clearly discussed in the book by Mei (1989, pp. 59–66), the perturbation approach used by Lau & Travis (1973) is strictly valid when the ratio $\beta L^*/h_0^*$ is much smaller than one. Herein β denotes the beach slope and h_0^* is a characteristic value of the water depth. For intermediate depths, the assumption $\beta L^*/h_0^* \ll 1$ is not particularly restrictive, since actual values of the beach slope are small. However, close to the beach, where the water depth turns out to be much smaller than the wavelength of the wavefield, in order to apply the approach of Lau & Travis (1973), it is necessary to consider very small values of β. Indeed, from the assumption $\beta L^*/h_0^* \ll 1$, it follows that $\beta \ll h_0^*/L^*$. Since $h_0^*/L^* \ll 1$, it turns out that close to the beach, the approach of Lau & Travis (1973) can only be applied for rather small values of β.

In this paper an attempt is made to predict the shoaling process of a wave propagating on a gently sloping bottom and partly reflected at the coastline. In particular, attention is focused on the study of the steady-velocity components. Since we consider the region close to the coast, the water depth is assumed to be much smaller than the length of the waves and the shallow-water approximation is used. For the consistency of the analysis, the beach slope β is assumed to be of order h_0^*/L^*, i.e. $\beta = \beta_0 h_0^*/L^*$ with β_0 of order one. Moreover, waves of small amplitudes with respect to the local depth are considered. The Reynolds number is assumed to be large and the flow regime in the bottom boundary layer to be laminar. Close to the bottom the results by Longuet-Higgins (1953) and Hunt & Johns (1963) are recovered. Far from the bottom, in the so-called 'core' region, our approach allows us to predict the local wave amplitude and the steady-velocity components. To compute them, an advection–diffusion equation for the vorticity field is solved. As discussed by Longuet-Higgins (1953), the solution depends on the ratio a^*/δ^* between the wave amplitude and the thickness of the bottom boundary layer. When this ratio is much smaller than one, the creeping-flow approximation can be used and the solution can be easily worked out by analytical means. For values of a^*/δ^* of order one or much larger than one, convection of vorticity is of the same order of magnitude or even

larger than vorticity diffusion. In the latter case, large normal gradients of vorticity develop near to the bottom to balance the governing equations and compensate for the smallness of δ^* with respect to a^*. The steady vorticity then remains confined within an outer boundary layer often referred to as the 'Stuart layer', which is close to the Stokes layer and may leave the bottom for highly reflected waves. In these cases a numerical approach should be used to solve the vorticity equation.

The knowledge of the steady currents generated far from the bottom by wave propagation is particularly relevant for morphodynamics models. Indeed, it is generally accepted (cf. Fredsøe & Deigaard 1992) that waves propagating over an erodible fine-sand bed generate a sediment suspension with large concentration in the near-bed region. When currents (in this case wave-generated currents) are present, additional mixing over the water depth occurs, resulting in an increase in the sediment concentration in the upper layers. Measurements in wave flumes show in particular the presence of sediments up to the water surface (Van Rijn 1990, 1993). The basic mechanism of sediment transport in combined currents and waves is thus the entrainment of particles by the stirring action of waves and their transport by the current. The present analysis assumes a laminar regime. The extension to the turbulent regime does not imply additional problems once an appropriate turbulence model is chosen. A first attempt to take into account turbulent effects has been done by Blondeaux *et al*. (1999), who compared the theoretical results with available field data and obtained a fair agreement even though some discrepancies were also found. To obtain a more accurate description of field conditions, more refined turbulence models than that of Blondeaux *et al*. (1999) should be used and the analysis should be extended to describe irregular waves. It is likely that the presence of many wave components leads to weaker steady streaming and a partial disappearance of the regular recirculating cells which are found for highly reflective beaches.

We conclude this introduction by pointing out that the recent experimental and theoretical investigations of Matsunaga *et al*. (1988, 1994) and Li & Dalrymple (1998) have shown that the undertow may be unstable and gives rise to seaward-migrating vortices with shorter length-scales and longer time-scales than the wavefield. However, this aspect of the phenomenon is not presently considered.

The procedure used in the rest of the paper is as follows. In the next section we formulate the problem. In § 3 the oscillatory part of the solution describing a monochromatic gravity wave propagating on a sloping bottom is obtained both in the outer region and in the bottom boundary layer. The steady-velocity components are determined in § 4. The results are described in § 5, while § 6 is devoted to the main conclusions of the work.

2. Formulation of the problem

Let us consider a coastal region uniform in the longshore direction and characterized by a constant sloping bottom (see figure 1). The flow is supposed to be forced by a monochromatic sea wave of angular frequency ω^* which normally approaches the coast and is partly reflected at the beach (hereafter a star denotes a dimensional quantity).

We introduce a Cartesian coordinate system with the x^*- and z^*-axes lying on the still-water level and pointing in the offshore and longshore directions, respectively,

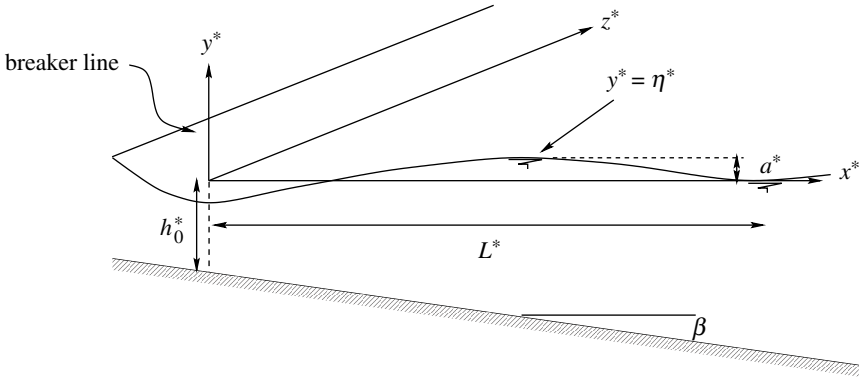

Figure 1. Sketch of the adopted coordinates and length-scales.

such that the $x^* = 0$ is a cross-shore location just offshore of the breaker line (see figure 1).

The local water depth h^*, which increases in the seaward direction at a constant rate β starting from a finite value h_0^* at $x^* = 0$, is described by the relationship

$$h^* = h_0^* + \beta x^*. \tag{2.1}$$

By assuming that the wavefield forced by the incoming wave is uniform in the long-shore direction, the problem of studying the velocity field is posed in terms of the continuity equation along with momentum equations in both the cross-shore and vertical directions.

The problem is then closed by the no-slip condition at the bottom, which forces the vanishing of the velocity, and by the kinematic and dynamic conditions at the free surface, which is assumed to be described by

$$y^* = \eta^*(x^*, t^*). \tag{2.2}$$

With the assumption that the horizontal length-scale of the problem

$$L^* = \sqrt{g^* h_0^*}/\omega^*$$

is much larger than the local depth, continuity and momentum equations along with boundary conditions can be simplified. Let us introduce the following dimensionless variables,

$$x = \frac{x^*}{L^*}, \qquad y = \frac{y^*}{h_0^*}, \qquad t = \omega^* t^*, \tag{2.3}$$

$$u = \frac{u^*}{a^*\omega^* L^*/h_0^*}, \qquad v = \frac{v^*}{a^*\omega^*}, \qquad p = \frac{p^*}{\rho^* g^* a^*}, \qquad \eta = \frac{\eta^*}{a^*}, \tag{2.4}$$

where t^* is the time, u^* and v^* denote the velocity components along the x^*- and y^*-axes, respectively, and p^* is the pressure. Moreover, ρ^* denotes the density of the sea water and $\mu^* = \nu^*\rho^*$ its dynamic viscosity, and a^* is a measure of the wave amplitude which is specified in the following.

Then, if the ratio h_0^*/L^* is assumed to be much smaller than one (strictly infinitesimal) and the dynamic pressure P is introduced,

$$P = p + \left(\frac{y}{a} - \eta\right), \tag{2.5}$$

the problem is posed by equations

$$\frac{\partial u}{\partial x}+\frac{\partial v}{\partial y}=0, \tag{2.6}$$

$$\frac{\partial u}{\partial t}+a\left[u\frac{\partial u}{\partial x}+v\frac{\partial u}{\partial y}\right]=-\frac{\partial \eta}{\partial x}-\frac{\partial P}{\partial x}+\tfrac{1}{2}\delta^2\frac{\partial^2 u}{\partial y^2}, \tag{2.7}$$

$$\frac{\partial P}{\partial y}=0, \tag{2.8}$$

along with the boundary conditions

$$u=0, \quad \beta_0 u+v=0 \quad \text{at } y=-h, \tag{2.9}$$

$$\frac{\partial \eta}{\partial t}+au\frac{\partial \eta}{\partial x}-v=0 \quad \text{at } y=a\eta, \tag{2.10}$$

$$P=0 \quad \text{at } y=a\eta, \tag{2.11}$$

$$\frac{\partial u}{\partial y}=0 \quad \text{at } y=a\eta. \tag{2.12}$$

The main steps which are necessary to derive equations (2.5)–(2.8) are outlined, for example, in Peregrine (1967). For convenience, the vanishing of the velocity at the bottom is enforced by stating that both the normal and the tangential velocity components must vanish. Use of (2.9) allows for an easy forcing of the no-slip condition when studying the flow in the bottom boundary layer, where use is made of the velocity components normal and tangential to the bottom. The boundary condition (2.10) is obtained by assuming the free surface to be a material surface. Finally, conditions (2.11) and (2.12) come from the continuity of the pressure and of the shear stress through the free surface when both surface tension and wind stresses are negligible.

The problem is characterized by three parameters, namely

$$a=\frac{a^*}{h_0^*}, \quad \delta=\frac{\sqrt{2\nu^*/\omega^*}}{h_0^*} \quad \text{and} \quad \beta_0, \tag{2.13}$$

where ν^* is the kinematic viscosity of the sea water. The first parameter, which is related to the ratio between the wave amplitude and the water depth, measures the relevance of nonlinear effects. Offshore of the breaker line, a turns out to be small and nonlinear effects are weak. The parameter δ, which is the ratio between the thickness of the viscous bottom boundary layer and the water depth, measures the importance of viscous effects. In the field, δ is very small and viscous stresses are negligible apart from a region close to the bottom. Finally, the geometric parameter β_0 is related to the slope β of the sea bottom which should be of order h_0^*/L^* to make shallow-water approximation valid for x of order one:

$$\beta=\left(\frac{h_0^*}{L^*}\right)\beta_0, \tag{2.14}$$

β_0 being of order one.

Equation (2.8), along with boundary condition (2.11), simply states that P identically vanishes. Hence, in the following we look for the solution of (2.6), (2.7) forced by

an incoming wave which is partly reflected at the beach and subject to (2.9), (2.10), (2.12). In particular, as pointed out in § 1, we determine the steady-velocity components which are necessary to evaluate the mass transport induced by the incoming wave. As discussed in the literature (e.g. Mei 1989, pp. 504–512), the validity of (2.6)–(2.12) simply implies $h_0^*/L^* \ll 1$.

3. The wavefield

In order to determine the wavefield, we consider amplitudes of the incoming wave much smaller than the local depth, such that the parameter a is much smaller than one. It is thus possible to expand the solution in the form

$$(u, v, \eta) = (u_0, v_0, \eta_0) + a(u_1, v_1, \eta_1) + O(a^2). \tag{3.1}$$

Since we retain terms of order $a = a^*/h_0^*$ in the expansion (3.1), while we drop terms of order h_0^*/L^*, at this stage the analysis requires that $h_0^*/L^* \ll a^*/h_0^*$. However, later on (see § 4) it is required that h_0^*/L^* be much smaller than $(a^*/h_0^*)^2$; hence the analysis holds when the ratio $U_r = a^*(L^*)^2/(h_0^*)^3$, also known as the Ursell number, is much larger than one.

When (3.1) is substituted into (2.6)–(2.12), we readily find that the following equations and boundary conditions should be satisfied at the leading order of approximation:

$$\frac{\partial u_0}{\partial x} + \frac{\partial v_0}{\partial y} = 0, \tag{3.2}$$

$$\frac{\partial u_0}{\partial t} = -\frac{\partial \eta_0}{\partial x} + \tfrac{1}{2}\delta^2 \frac{\partial^2 u_0}{\partial y^2}, \tag{3.3}$$

$$u_0 = 0, \quad \beta_0 u_0 + v_0 = 0 \quad \text{at } y = -h, \tag{3.4}$$

$$\frac{\partial \eta_0}{\partial t} - v_0 = 0 \quad \text{at } y = 0, \tag{3.5}$$

$$\frac{\partial u_0}{\partial y} = 0 \quad \text{at } y = 0. \tag{3.6}$$

The problem for (u_0, v_0, η_0) contains the parameter δ, which field data show to be much smaller than one. Hence, it is possible to assume

$$(u_0, v_0, \eta_0) = (u_{00}, v_{00}, \eta_{00}) + O(\delta). \tag{3.7}$$

Since the perturbation parameter δ multiplies the highest-order derivative, it is necessary to split the y-domain into two parts: a boundary layer close to the bottom, the thickness of which is of order δ; and a core region in which y assumes values of order one. In the former region viscous effects are relevant, while they are negligible in the core region as the oscillatory character of the flow keeps vorticity confined within the bottom boundary layer and the fluid in the core region behaves as an inviscid fluid. These balances between viscous effects and local inertia take place at the leading order of approximation in the parameter a. In § 4 it is shown that at the following order of approximation ($O(a)$), viscosity can play a significant role even in the core region depending on the ratio between a^* and δ^*. This is a well-known phenomenon discussed in detail in the literature (see, for example, Mei 1989, pp. 439–443).

If a monochromatic wave approaches the coast, the linearity of (3.2)–(3.6) suggests that we assume that

$$(u_{00}, v_{00}, \eta_{00}) = (\hat{u}_{00}(x,y), \hat{v}_{00}(x,y), \hat{\eta}_{00}(x,y))\mathrm{e}^{\mathrm{i}t} + \text{c.c.} \tag{3.8}$$

Then equation (3.3), without the negligible viscous term, implies

$$\hat{u}_{00} = \mathrm{i}\frac{\mathrm{d}\hat{\eta}_{00}}{\mathrm{d}x}, \tag{3.9}$$

while (3.2), along with (3.5) and (3.9), leads to

$$\hat{v}_{00} = -\mathrm{i}y\frac{\mathrm{d}^2\hat{\eta}_{00}}{\mathrm{d}x^2} + \mathrm{i}\hat{\eta}_{00}. \tag{3.10}$$

Finally, substitution of (3.9) and (3.10) into (3.4) leads to an ordinary differential equation for $\hat{\eta}_{00}$ which can be easily solved if the variable $X = 1 + \beta_0 x$ is introduced:

$$\hat{\eta}_{00} = \tfrac{1}{2}H_0^{(1)}\left(\frac{2\sqrt{X}}{\beta_0}\right) + \hat{K}\tfrac{1}{2}H_0^{(2)}\left(\frac{2\sqrt{X}}{\beta_0}\right). \tag{3.11}$$

In (3.11) $H_0^{(1)}$, $H_0^{(2)}$ are the Hankel functions (Abramowitz & Stegun 1964). The complex reflection coefficient $\hat{K}$ of the beach is introduced to also model waves partly reflected at the coastline. The modulus of $\hat{K}$ is related to the ratio between the amplitude of the reflected wave and that of the incident wave. The phase of $\hat{K}$ is related to the relative phase of the incoming and outgoing waves. The range of validity of (3.11) is discussed in Friedricks (1948) for vanishing values of h_0^* and a fully reflected wave. In this case, if we consider a beach geometry characterized by β of order 10^{-2} a comparison of (3.11) with the solution of the full three-dimensional problem (Stoker 1957) shows that (3.11) is valid within a nearshore region the width of which is about seven wavelengths. Values of β of order 10^{-2} have been chosen on the basis of the analysis of a large number of beach profiles surveyed at the Field Research Facility, Duck, NC. Although different values of β can be found all around the world and larger values of β imply a decrease in the range of validity of (3.11), it can be stated that (3.11) provides reasonable results even for field conditions. It is interesting to point out that in (3.11) the wave amplitude changes only because of the varying water depth. Indeed the viscous damping of the wave amplitude is present only when terms of order δ are included in (3.7) and induces a significant change of the wave amplitude only on a spatial scale much larger than L^*. Since the present analysis considers a coastal region of order L^*, it is not necessary to include $O(\delta)$ terms in (3.11).

At this stage it is possible to introduce a more precise definition of a^*. Because of (3.11) and of the dimensionless variable η defined by (2.4), a^* is the amplitude of the incoming wave at $x^* = 0$ divided by $|H_0^{(1)}(2/\beta_0)|$.

Of course, functions $\hat{u}_{00}$ and $\hat{v}_{00}$ do not satisfy the boundary conditions at the bottom, because they have been obtained by neglecting viscous term in (3.3). As previously pointed out, in order to satisfy the no-slip condition at the bottom, it is necessary to introduce a boundary layer, the thickness of which is of $O(\delta)$. Hence, in order to determine the flow inside the bottom boundary layer it is convenient to rescale the vertical coordinate by introducing a variable ξ such that

$$\xi = \frac{y + h(x)}{\delta}, \tag{3.12}$$

and to define $\hat{U}_{00}$, $\hat{V}_{00}$ such that

$$\hat{U}_{00} = \hat{u}_{00}, \qquad \hat{V}_{00} = \frac{1}{\delta}(\hat{v}_{00} + \beta_0 \hat{u}_{00}). \tag{3.13}$$

The solution of the problem inside the boundary layer gives

$$\hat{U}_{00} = \mathrm{i}\frac{\mathrm{d}\hat{\eta}_{00}}{\mathrm{d}x}[1 - \mathrm{e}^{-(1+\mathrm{i})\xi}], \tag{3.14}$$

$$\hat{V}_{00} = -\mathrm{i}\frac{\mathrm{d}^2\hat{\eta}_{00}}{\mathrm{d}x^2}\left[\xi + \frac{1}{(1+\mathrm{i})}(\mathrm{e}^{-(1+\mathrm{i})\xi} - 1)\right]. \tag{3.15}$$

The function $\hat{U}_{00}$ for ξ tending to infinity exactly matches the function $\hat{u}_{00}$ for y tending to $-h$. Moreover, making use of relationships obtained for the flow in the core region, it can be shown that the first term on the right-hand side of (3.15) matches $\hat{v}_{00}$ for y tending to $-h$. For ξ tending to infinity, the second term on the right-hand side of (3.15) is not balanced by any terms in (3.10) but produces a forcing in the problem at order δ. This problem can be solved only when a solvability condition is satisfied. As discussed in Vittori & Blondeaux (1996), this solvability condition requires that the amplitudes of both the incoming and the reflected waves depend on a slow coordinate, i.e. the dimensional amplitudes change on a spatial scale $L^* h_0^*/\delta^*$ much larger than the length of the incoming wave. Since we focus our attention on a region near to the shore, the cross-shore width of which scales with L^*, the slow variations of the amplitudes can be neglected and the details of the $O(\delta)$-problem are not given here.

4. The steady currents

The solution obtained so far describes a long wave propagating on slowly varying depths.

In order to determine the steady-velocity components, it is necessary to move to the following order of approximation, i.e. to $O(a)$. Because of nonlinear effects, the $O(a)$ terms in (3.1) should contain both a part proportional to $\mathrm{e}^{2\mathrm{i}t}$ and a steady part:

$$u_1 = \hat{u}_1 \mathrm{e}^{2\mathrm{i}t} + \bar{u}_1 + \text{c.c.}, \tag{4.1}$$

$$v_1 = \hat{v}_1 \mathrm{e}^{2\mathrm{i}t} + \bar{v}_1 + \text{c.c.}, \tag{4.2}$$

$$\eta_1 = \hat{\eta}_1 \mathrm{e}^{2\mathrm{i}t} + \bar{\eta}_1 + \text{c.c.} \tag{4.3}$$

Since our aim is to predict the mass-transport velocity, we focus our attention on the latter contribution.

Continuity and momentum equations for the flow in the core region are

$$\frac{\partial \bar{u}_1}{\partial x} + \frac{\partial \bar{v}_1}{\partial y} = 0, \tag{4.4}$$

$$\frac{\partial \bar{\eta}_1}{\partial x} = -\frac{\partial}{\partial x}(\overline{\tfrac{1}{2}u_{00}^2}), \tag{4.5}$$

subject to the boundary conditions

$$\beta_0\bar{u}_1 + \bar{v}_1 = 0 \quad \text{at } y = -(1+\beta_0 x), \tag{4.6}$$

$$\bar{v}_1 = \overline{u_{00}\frac{\partial \eta_{00}}{\partial x}} - \overline{\eta_{00}\frac{\partial v_{00}}{\partial y}} \quad \text{at } y = 0, \tag{4.7}$$

$$\frac{\partial \bar{u}_1}{\partial y} = 0 \quad \text{at } y = 0, \tag{4.8}$$

and to the matching condition with the solution valid in the bottom boundary layer. Equations (4.4), (4.5) and boundary conditions (4.6)–(4.8) are obtained by substituting (3.1) and (4.1)–(4.3) into (2.5)–(2.12), considering terms of $O(a)$ and performing a time average over the wave period which hereinafter is indicated by an overbar.

The assumptions previously introduced allow us to conclude that at $O(a)$ viscous terms in the momentum equation are negligible in the core region. Indeed the term

$$\tfrac{1}{2}\delta^2\frac{\partial^2 \bar{u}_1}{\partial y^2}$$

is much smaller than any of the terms appearing in (4.5) and the term

$$\tfrac{1}{2}\delta^2\frac{\partial^2 u_0}{\partial y^2},$$

which might appear at $O(a)$, depending on the value of the ratio a/δ^2, identically vanishes. Notwithstanding that viscous terms do not appear in (4.5), viscosity may affect the velocity field $(\bar{u}_1, \bar{v}_1)$ in the core region. In fact in the following it is shown that, depending on the ratio a/δ, viscosity may control the spatial distribution of the steady vorticity component in the whole water column and hence also the values of $(\bar{u}_1, \bar{v}_1)$, which cannot be determined only by means of (4.4), (4.5) (see Longuet-Higgins 1953).

Inside the bottom boundary layer, it is convenient to introduce the quantities

$$\bar{U}_1 = \bar{u}_1, \qquad \bar{V}_1 = \frac{1}{\delta}(\bar{v}_1 + \beta_0\bar{u}_1), \tag{4.9}$$

which should satisfy the following equations,

$$\frac{\partial \bar{U}_1}{\partial x} + \frac{\partial \bar{V}_1}{\partial \xi} = 0, \tag{4.10}$$

$$\frac{\partial^2 \bar{U}_1}{\partial \xi^2} = 2\left[\frac{\partial \bar{\eta}_1}{\partial x} + \overline{U_{00}\frac{\partial U_{00}}{\partial x}} + \overline{V_{00}\frac{\partial U_{00}}{\partial \xi}}\right], \tag{4.11}$$

along with the boundary conditions

$$\bar{U}_1 = 0, \quad \bar{V}_1 = 0 \quad \text{for } \xi = 0, \tag{4.12}$$

and the matching condition with the solution in the core region.

The values of $\bar{U}_1$ and $\bar{V}_1$ can be easily derived, if (4.5) is used. In particular,

$$\bar{U}_1 = \frac{\mathrm{d}\hat{\eta}_{00}}{\mathrm{d}x}\left(\frac{\mathrm{d}^2\hat{\eta}_{00}}{\mathrm{d}x^2}\right)^{\dagger}\{[(1+3\mathrm{i}) - (1-\mathrm{i})\xi]\mathrm{e}^{-(1+\mathrm{i})\xi} - \mathrm{i}\mathrm{e}^{-(1-\mathrm{i})\xi} + \tfrac{1}{2}(1-\mathrm{i})\mathrm{e}^{-2\xi} - \tfrac{3}{2}(1+\mathrm{i})\}, \tag{4.13}$$

which is the result of interest here. In (4.13) the symbol $()^\dagger$ denotes the complex conjugate of a complex quantity.

As already pointed out, the evaluation of the steady cross-shore velocity component in the core region cannot be performed by simply considering (4.4), which is the only available equation for the two unknowns $\bar{u}_1$ and $\bar{v}_1$. As also discussed by Longuet-Higgins (1953) one further relationship must be given by considering the behaviour of the vorticity Ω^*, which is defined by

$$\Omega^* = \frac{\partial v^*}{\partial x^*} - \frac{\partial u^*}{\partial y^*}. \tag{4.14}$$

Vorticity dynamics is controlled by the vorticity equation, which in dimensionless form reads

$$\frac{\partial \Omega}{\partial t} + a\left[u\frac{\partial \Omega}{\partial x} + v\frac{\partial \Omega}{\partial y}\right] = \tfrac{1}{2}\delta^2 \frac{\partial^2 \Omega}{\partial y^2}. \tag{4.15}$$

Cross-shore diffusion is neglected in (4.15) because of the shallow-water approximation, which leads us also to state that

$$\Omega \cong -\frac{\partial u}{\partial y}. \tag{4.16}$$

Since the parameter a is small, it is appropriate to expand Ω in terms of a. Moreover, the interaction of the different temporal components gives rise to the following form of Ω:

$$\begin{aligned}\Omega &= \Omega_0 + a\Omega_1 + a^2\Omega_2 + O(a^3)\\ &= [\hat{\Omega}_0 \mathrm{e}^{\mathrm{i}t} + \text{c.c.}] + a[\bar{\Omega}_1 + \hat{\Omega}_1 \mathrm{e}^{2\mathrm{i}t} + \text{c.c.}] + a^2[(\hat{\Omega}_{21}\mathrm{e}^{\mathrm{i}t} + \hat{\Omega}_{23}\mathrm{e}^{3\mathrm{i}t}) + \text{c.c.}] + O(a^3).\end{aligned} \tag{4.17}$$

For (4.17) to be meaningful, it is necessary that the $O(h_0^*/L^*)$ term neglected in (4.16) be much smaller than the smallest term retained in (4.17). Hence, h_0^*/L^* should be much smaller than $(a^*/h_0^*)^2$. As already discussed in § 3 this implies that the Ursell number should be much larger than one.

At the leading order of approximation, in the core region the vorticity vanishes, i.e. $\hat{\Omega}_0 \equiv 0$. By substituting (4.17) into (4.15) and by analysing the vorticity equation at orders a and a^2, it turns out that the oscillating part of Ω_1 vanishes (i.e. $\hat{\Omega}_1 = 0$) along with the part of Ω_2 proportional to $\mathrm{e}^{3\mathrm{i}t}$ (i.e. $\hat{\Omega}_{23} = 0$). Moreover, it follows that

$$\hat{\Omega}_{21} = \mathrm{i}\left[\hat{u}_0\frac{\partial \bar{\Omega}_1}{\partial x} + \hat{v}_0\frac{\partial \bar{\Omega}_1}{\partial y}\right]. \tag{4.18}$$

Therefore, the steady part of the vorticity equation reads

$$\begin{aligned}\tfrac{1}{2}\delta^2 a\frac{\partial^2 \bar{\Omega}_1}{\partial y^2} = a^3\Bigg\{\bar{u}_1\frac{\partial \bar{\Omega}_1}{\partial x} + \bar{v}_1\frac{\partial \bar{\Omega}_1}{\partial y} + \Bigg[\mathrm{i}\hat{u}_{00}^\dagger\frac{\partial}{\partial x}\left(\hat{u}_{00}\frac{\partial \bar{\Omega}_1}{\partial x} + \hat{v}_{00}\frac{\partial \bar{\Omega}_1}{\partial y}\right) +\\ + \mathrm{i}\hat{v}_{00}^\dagger\frac{\partial}{\partial y}\left(\hat{u}_{00}\frac{\partial \bar{\Omega}_1}{\partial x} + \hat{v}_{00}\frac{\partial \bar{\Omega}_1}{\partial y}\right) + \text{c.c.}\Bigg]\Bigg\} + \text{h.o.t.}\end{aligned} \tag{4.19}$$

(where 'h.o.t.' denotes higher-order terms), or, with straightforward algebra,

$$\frac{\partial^2\bar{\Omega}_1}{\partial y^2} = 2\left(\frac{a}{\delta}\right)^2\left\{\bar{u}_1\frac{\partial\bar{\Omega}_1}{\partial x} + \bar{v}_1\frac{\partial\bar{\Omega}_1}{\partial y} + \left[\mathrm{i}\hat{u}_{00}^{\dagger}\frac{\partial\hat{u}_{00}}{\partial x}\frac{\partial\bar{\Omega}_1}{\partial x} + \mathrm{i}\left(\hat{u}_{00}^{\dagger}\frac{\partial\hat{v}_{00}}{\partial x} + \hat{v}_{00}^{\dagger}\frac{\partial\hat{v}_{00}}{\partial y}\right)\frac{\partial\bar{\Omega}_1}{\partial y} + \mathrm{c.c.}\right]\right\} + \mathrm{h.o.t.} \tag{4.20}$$

As discussed by Dore (1976), the equation for the steady part of the vorticity turns out to be of convection–diffusion type with further terms given by the interaction of the first-order oscillatory solution with itself and with the steady vorticity field (see contributions to (4.20) within square brackets).

The solution of (4.20) depends on the values assumed by the ratio between δ and a. When the wave amplitude is much smaller than the Stokes layer thickness, the creeping-flow approximation can be used. While unrealistic in practical situations this approximation is the easiest to analyse. In fact, from (4.20), it follows that the steady vorticity component varies linearly with the water depth while the steady velocity is quadratic. Then, boundary conditions (4.6)–(4.8) allow for $\bar{u}_1$ to be determined:

$$\bar{u}_1 = \frac{3}{2X}\frac{\mathrm{d}\hat{\eta}_{00}}{\mathrm{d}X}\beta_0\left\{\left(\frac{y}{X}\right)^2\left[-\tfrac{3}{2}X(1+\mathrm{i})\beta_0^2\left(\frac{\mathrm{d}^2\hat{\eta}_{00}}{\mathrm{d}X^2}\right)^{\dagger} + \mathrm{i}(\hat{\eta}_{00})^{\dagger}\right] + \tfrac{1}{2}X(1+\mathrm{i})\beta_0^2\left(\frac{\mathrm{d}^2\hat{\eta}_{00}}{\mathrm{d}X^2}\right)^{\dagger} - \mathrm{i}(\hat{\eta}_{00})^{\dagger}\right\}. \tag{4.21}$$

When the ratio δ/a is of order one, all terms of equation (4.20) should be retained. Therefore, only a numerical procedure can provide the solution. If the wave amplitude is much larger than the thickness of the Stokes layer, viscosity is negligible except within a bottom layer. Vorticity is expected to be confined within this second boundary layer, which turns out to be adjacent to the Stokes bottom boundary layer, and to diminish to zero outside it (Stuart 1966). Since in the second boundary layer, the solution should be found numerically, the cases $a \gg \delta$ and $a \sim \delta$ are treated together. To numerically solve equation (4.20), the variables X and Y which map the flow domain into a rectangle are introduced:

$$X = 1 + \beta_0 x, \qquad Y = \frac{y}{1+\beta_0 x}. \tag{4.22}$$

Moreover, the stream function $\bar{\psi}_1$ is introduced such that

$$\bar{u}_1 = \frac{\partial\bar{\psi}_1}{\partial y} \quad \text{and} \quad \bar{v}_1 = -\frac{\partial\bar{\psi}_1}{\partial x}.$$

It turns out that

$$\frac{\partial^2\bar{\Omega}_1}{\partial Y^2} - 2\beta_0 X\left(\frac{a}{\delta}\right)^2\left\{\frac{\partial\bar{\psi}_1}{\partial Y}\frac{\partial\bar{\Omega}_1}{\partial X} - \frac{\partial\bar{\psi}_1}{\partial X}\frac{\partial\bar{\Omega}_1}{\partial Y} + \left[X\frac{\partial\bar{\Omega}_1}{\partial X} - Y\frac{\partial\bar{\Omega}_1}{\partial Y}\right]\left[\mathrm{i}\beta_0^3\left(\frac{\mathrm{d}\hat{\eta}_{00}}{\mathrm{d}X}\right)^{\dagger}\frac{\mathrm{d}^2\hat{\eta}_{00}}{\mathrm{d}X^2} + \mathrm{c.c.}\right] - \frac{\partial\bar{\Omega}_1}{\partial Y}\left[\mathrm{i}\left(\beta_0^3\left(\frac{\mathrm{d}\hat{\eta}_{00}}{\mathrm{d}X}\right)^{\dagger}\frac{\mathrm{d}^3\hat{\eta}_{00}}{\mathrm{d}X^3}YX + \beta_0(\hat{\eta}_{00})^{\dagger}\frac{\mathrm{d}^2\hat{\eta}_{00}}{\mathrm{d}X^2}\right) + \mathrm{c.c.}\right]\right\} = 0, \tag{4.23}$$

$$\frac{\partial^2 \bar{\psi}_1}{\partial Y^2} = -X^2 \bar{\Omega}_1. \tag{4.24}$$

With straightforward algebra it can be verified that (4.23) leads to

$$\frac{\partial^2 \bar{\Omega}_1}{\partial Y^2} - 2\beta_0 X \left(\frac{a}{\delta}\right)^2 \left\{ \frac{\partial \bar{\psi}_1}{\partial Y}\frac{\partial \bar{\Omega}_1}{\partial X} - \frac{\partial \bar{\psi}_1}{\partial X}\frac{\partial \bar{\Omega}_1}{\partial Y} + \left[\mathrm{i}\beta_0 (\hat{\eta}_{00})^\dagger \frac{\mathrm{d}\hat{\eta}_{00}}{\mathrm{d}X} + \text{c.c.} \right] \left[\frac{\partial \bar{\Omega}_1}{\partial X} + \frac{1+Y}{X}\frac{\partial \bar{\Omega}_1}{\partial Y} \right] \right\} = 0. \tag{4.25}$$

Then the vertical coordinate Y is stretched by introducing the variable $\hat{Y}$, to better describe the large gradients which are present close to $Y = -1$ when a becomes much larger than δ:

$$\hat{Y} = \ln\left(\frac{c+1+Y}{c}\right). \tag{4.26}$$

In (4.26) the value of the stretching parameter c should be properly chosen. Finally, equations (4.24) and (4.25) are solved by means of a finite-difference approach which uses a second-order centred scheme to approximate the $\hat{Y}$-derivatives and a first-order upwind scheme for the X-derivatives. The solution is found by an iterative procedure after introducing a fictitious time-derivative term into (4.25) which is used to update the values of $\bar{\Omega}_1$, while (4.24) is used to compute $\bar{\psi}_1$ and hence $\bar{u}_1$ and $\bar{v}_1$ (Roache 1972). The vorticity and stream function behaviours described in the following are obtained by using a number of grid points which depends on the parameters of the problem and ranges from 100 to 300 and from 100 to 1200 in the horizontal and vertical directions, respectively. The same cases have been run doubling the number of grid points both in the horizontal and vertical directions and using different values of the stretching parameter c appearing in (4.26). The results obtained in this second set of runs are coincident with those reported in the following. Moreover, different time-steps have been used but the final solution turns out to be independent of the time-step employed. These findings ensure both reliability and accuracy of the numerical procedure and of the obtained results. It is worth pointing out that the solution of (4.24) and (4.25) can be determined only when appropriate boundary conditions are specified. At the free surface ($Y = 0$) the vanishing of the tangential stress (4.8) forces

$$\bar{\Omega}_1 = 0 \quad \text{at } Y = 0. \tag{4.27}$$

Moreover, the kinematic boundary condition (4.7) leads to

$$\bar{\psi}_1 = -\mathrm{i}\beta_0 \frac{\mathrm{d}\hat{\eta}_{00}}{\mathrm{d}X}(\hat{\eta}_{00})^\dagger + \text{c.c.} \quad \text{at } Y = 0. \tag{4.28}$$

It is easy to verify (see § 5) that the boundary condition (4.28) is equivalent to requiring the vanishing of the time-averaged mass flux at any cross-shore section.

The matching of the flow in the core region with that in the bottom boundary layer implies

$$\frac{\partial \bar{\psi}_1}{\partial Y} = -\tfrac{3}{2}(\mathrm{i}+1)X\beta_0^3 \frac{\mathrm{d}\hat{\eta}_{00}}{\mathrm{d}X}\frac{\mathrm{d}^2(\hat{\eta}_{00})^\dagger}{\mathrm{d}X^2} + \text{c.c.} \quad \text{at } Y = -1, \tag{4.29}$$

$$\bar{\psi}_1 = 0 \quad \text{at } Y = -1. \tag{4.30}$$

It is worth pointing out that the boundary condition (4.29) has been converted into a boundary condition for the vorticity $\bar{\Omega}_1$ following a procedure similar to that suggested by Thom (1928) and discussed, for example, in Roache (1972).

Finally, a boundary condition should be given at some cross-shore location. This raises a difficult question regarding both the type of boundary condition which must be applied and the location in which it must be forced.

The simplest case is that of a standing wave generated by the full reflection of an incoming wave at a vertical wall located somewhere between $0 < X \leqslant 1$. Indeed at the wall or under the antinodes of the free-surface oscillations, no mass flux should be present and $\bar{u}_1$ should vanish. Moreover, from the definition of the stream function and of the vorticity, it follows that both $\bar{\psi}_1$ and $\bar{\Omega}_1$ should be zero under the antinodes, if the constant appearing in the definition of the stream function is properly chosen.

For a progressive or a partly reflected wave, since diffusion in the X-direction is neglected because of the use of the shallow-water approximation, it can only be stated that a boundary condition should be forced where the flow enters the computational domain. This physical and mathematical constraint is well modelled by the use of the upwind finite-difference scheme to approximate the X-derivatives. Indeed this scheme implies the forcing of a boundary condition only at the upstream boundaries of the computational domain. However, different boundary conditions can be used. A discussion of this issue can be found in the book by Roache (1972). The less-restrictive and convenient condition is that which forces the X-derivative of $\bar{\psi}_1$ to vanish. This constraint, already used in the 1960s to study the flow around cylinders or that induced by a backstep in a steady stream (e.g. Fromm 1963; Harlow & Fromm 1964; Thoman & Szewczyk 1966; Katsanis 1967), allows the stream function and the vorticity along the upstream boundary to develop as part of the computed solution and couples simplicity with efficiency. For a standing wave, the results obtained by forcing the vanishing of $\partial\bar{\psi}_1/\partial X$ have been compared with those derived by imposing the vanishing of $\bar{\psi}_1$ and good agreement has been found. Further support for the adopted boundary condition comes from the good agreement which has been found when the numerical code has been run for small values of a/δ and the results compared with (4.21). Although the specification of suitable boundary conditions at open boundaries is still an open question extensively discussed in the literature (see, for example, the Proceedings of the 'Open boundary conditions minisymposium' (Gresho & Sani 1990)), the above findings give us confidence in the suitability of the adopted boundary conditions.

5. Results

Since the thickness $\delta^* = \sqrt{2\nu^*/\omega^*}$ of the bottom boundary layer is much smaller than the length L^* of the incoming wave, the forms of both the oscillatory and the steady-velocity components close to the bottom do not differ from those determined by Longuet-Higgins (1953). Of course, as shown by Hunt & Johns (1963), to recover the results described by Longuet-Higgins (1953) it is necessary to scale the oscillatory velocity component with $|\hat{u}_{00}(x)| = |\mathrm{d}\hat{\eta}_{00}/\mathrm{d}x|$, which is the amplitude of the oscillations of the irrotational velocity induced locally close to the bottom by the propagating waves.

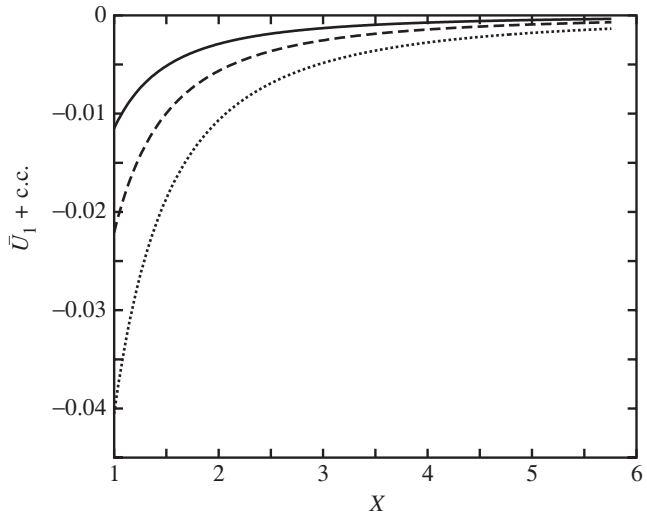

Figure 2. Influence of β_0 on the steady velocity at the top of the boundary layer for a fully absorbed wave at the coastline: solid line, $\beta_0 = 0.05$; dashed line, $\beta_0 = 0.1$; and dotted line, $\beta_0 = 0.2$.

On the other hand, equation (4.13) shows that the steady-velocity component should be scaled with

$$\hat{u}_{00}(x)\left(\frac{\mathrm{d}\hat{u}_{00}(x)}{\mathrm{d}x}\right)^{\dagger} = \left(\frac{\mathrm{d}\hat{\eta}_{00}}{\mathrm{d}x}\right)\left(\frac{\mathrm{d}^2\hat{\eta}_{00}}{\mathrm{d}x^2}\right)^{\dagger}.$$

Hence, at the first order of approximation, a Stokes boundary layer is generated close to the sea bed and the velocity oscillations depend on the strength of the local wavefield. Then nonlinear effects inside the viscous boundary layer give rise to a steady streaming, the intensity and direction of which depend on the characteristics of the propagating waves. When the reflection coefficient of the beach vanishes, i.e. no energy is reflected back from the beach towards the deep-water region, the steady-velocity component is shoreward directed whatever cross-shore location is considered and its strength increases while moving towards the shore. Of course the strength of the steady streaming also depends on the beach slope.

In figure 2 the constant value assumed by the steady-velocity component for ξ tending to infinity, i.e. at the top of the boundary layer, is plotted versus the cross-shore coordinate X for different values of β_0. As increasing values of β_0 are considered, the strength of the steady streaming increases more rapidly moving towards the beach. On the other side, when a fully reflective beach is considered, a standing wave is generated and the cross-shore steady-velocity component at the top of the bottom boundary layer is directed from the nodes towards the antinodes of the free-surface oscillations. Indeed from figure 3, where the value of $\bar{U}_1 + \text{c.c.}$ for ξ tending to infinity is plotted versus X, it can be seen that the steady-velocity component is alternatively negative and positive, i.e. shoreward and seaward directed, and the velocity is negative close to $x = 0$ ($X = 1$), where an antinode is located. It is worth pointing out that in figure 3 the phase of the reflected wave with respect to the incoming wave is chosen in such a way that the oscillating velocity component vanishes at $x = 0$, where a vertical wall is assumed to be located.

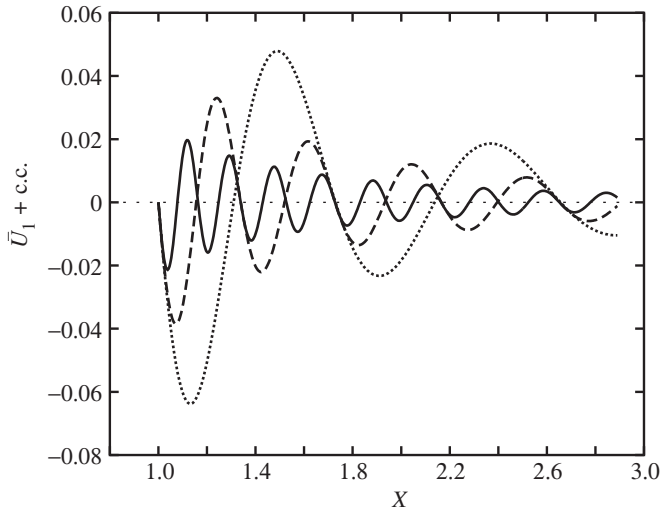

Figure 3. Influence of β_0 on the steady velocity at the top of the boundary layer for a fully reflected wave at the coastline: solid line, $\beta_0 = 0.05$; dashed line, $\beta_0 = 0.1$; and dotted line, $\beta_0 = 0.2$.

However, as clearly discussed in the book of Mei (1989, pp. 419–434), the steady-velocity components close to the bottom reverse their direction and are directed from the antinodes to the nodes of the free-surface oscillations. Hence, as discussed by Carter *et al.* (1973), Lau & Travis (1973) and Yu & Mei (2000), if the sediment particles are assumed to be small and move mainly by rolling and sliding along the sea bed (bed load), it follows that in the case of a fully reflected wave there is a net convergence of sediments under the nodes and a series of sand bars parallel to the coastline tend to form there. No plot of the vertical profile of $\bar{U}_1 + \text{c.c.}$ is provided because the behaviour of such a quantity versus ξ is that found by Longuet-Higgins and discussed by Carter *et al.* (1973).

Of course, the behaviour of the velocity close to the bottom can be investigated also for any value of $|\hat{K}|$ falling in the range $(0, 1)$. An example of the behaviour of $\bar{U}_1 + \text{c.c.}$ versus X at the top of the bottom boundary layer is plotted in figure 4 for $|\hat{K}| = 0.02$, 0.10, 0.50, and $\beta_0 = 0.05$. For the smallest value of $|\hat{K}|$ at the top of the bottom boundary layer the steady streaming is directed towards the coastline and monotonically increases when X tends to 1, even though small oscillations can be detected. When $|\hat{K}|$ is equal to 0.1, the effects of the reflected wave are more evident, although the steady-velocity component is always negative. For $|\hat{K}| = 0.5$ in a large part of the beach profile a shoreward-directed current is present, but cross-shore locations exist where a seaward-directed current is present.

Until now, as in Carter *et al.* (1973) and Lau & Travis (1973), the flow close to the sea bed has been discussed. These results are quite relevant to understand the morphological evolution of a beach profile when the sediment is supposed to move as bed load only. However, as pointed out in § 1, the combined action of waves and currents put into suspension a large amount of sediment, and sediment concentration may be relevant also near the sea surface. Therefore, in order to predict the total sediment transport, it is necessary to evaluate the steady-velocity components also in the core region, i.e. from the top of the bottom boundary layer up to the free surface.

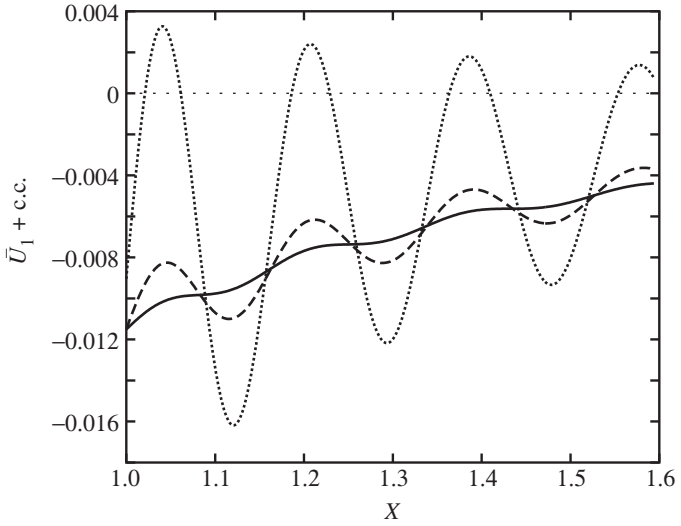

Figure 4. Influence of $|\hat{K}|$ on the patterns of the steady velocity at the top of the bottom boundary layer for $\beta_0 = 0.05$: solid line, $|\hat{K}| = 0.02$; dashed line, $|\hat{K}| = 0.1$; and dotted line, $|\hat{K}| = 0.5$.

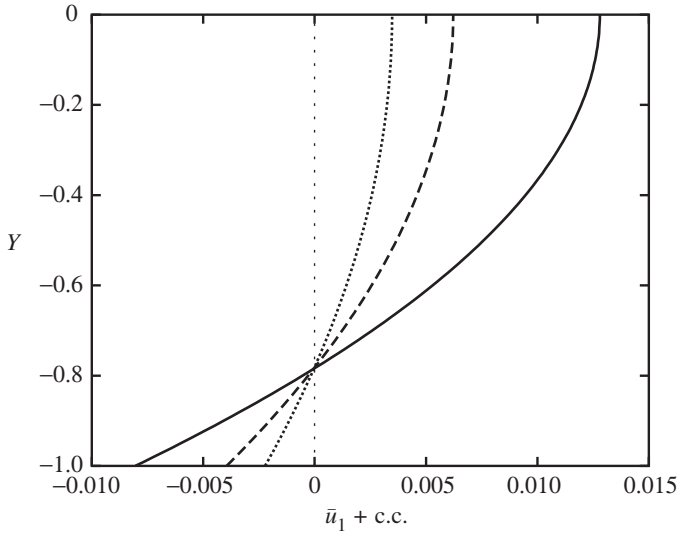

Figure 5. Vertical profiles of the cross-shore velocity for a fully absorbed wave and different cross-shore locations: solid line, $X = 2$; dashed line, $X = 3$; and dotted line, $X = 4$. Input parameters: $\beta_0 \simeq 0.16$, $\delta \simeq 0.008$ and $a = 0.002$.

When the thickness δ^* of the bottom boundary layer is much larger than the wave amplitude a^*, the creeping-flow approximation gives rise to a vertical velocity distribution which turns out to be parabolic. In figure 5 the cross-shore velocity component is shown at different cross-shore locations for an incoming wave which is fully absorbed at the coastline and for $\beta_0 \simeq 0.16$, $\delta \simeq 0.008$ and $a = 0.002$. As already pointed out, the velocity profile turns out to be parabolic and close to the

sea bottom the cross-shore velocity is shoreward directed. However, because of mass conservation, the depth-averaged value of $\bar{u}_1$ is seaward directed and decreases when moving offshore because of the increasing water depth. Indeed, at any cross-shore location the time average of the mass flux should vanish. In dimensionless form this condition reads

$$\frac{1}{2\pi}\int_t^{t+2\pi}\int_{-h}^{a\eta} u\,\mathrm{d}y\,\mathrm{d}t = 0. \tag{5.1}$$

By substituting (3.1) into (5.1) and splitting the integral over the vertical into two contributions, one from the bottom up to the still-water level and one from $y = 0$ to the free surface, it is easy to obtain

$$\frac{1}{2\pi}\int_t^{t+2\pi}\left[\int_{-h}^{0}(u_0 + a u_1)\,\mathrm{d}y + \int_0^{a\eta_0} u_0\,\mathrm{d}y\right]\mathrm{d}t + 0(a^2) = 0. \tag{5.2}$$

Since the functions $\hat{u}_0\mathrm{e}^{\mathrm{i}t} + \text{c.c.}$ and $\hat{u}_1\mathrm{e}^{2\mathrm{i}t} + \text{c.c.}$ are periodic with a vanishing time average, and given that the value of u_0 for $0 < y < a\eta_0$ can be approximated by $\hat{u}_0(0)\mathrm{e}^{\mathrm{i}t} + \text{c.c.}$ with an error of order a, it turns out that

$$\int_{-h}^{0}\bar{u}_1\,\mathrm{d}y + \hat{\eta}_0\hat{u}_0^{\dagger}|_{y=0} + \text{c.c.} = 0. \tag{5.3}$$

Hence, since the term $\hat{\eta}_0\hat{u}_0^{\dagger}|_{y=0} + \text{c.c.}$, which describes the shoreward-directed mass flux due to the oscillatory flow induced by the incoming wave, is negative, the term $\int_{-h}^{0}\bar{u}_1\,\mathrm{d}y$ must be positive, i.e. it must be seaward directed. Incidentally, it is worth pointing out that the fulfilment of (5.3) is assured by the kinematic boundary condition (4.28).

The results shown in figure 5 are for $\beta_0 \simeq 0.16$, $\delta \simeq 0.008$ and $a = 0.002$. Bearing in mind a laboratory experiment for an incoming wave characterized by a period of 2 s, the above values of the parameters imply $\beta \simeq 0.05$ and $h_0^* \simeq 0.10$ m. Moreover, the amplitude of the incoming wave at the shore turns out to be equal to 5×10^{-5} m. Similar unrealistic values of the wave amplitude are obtained whenever the dimensionless parameters are in the creeping-flow regime. These findings suggest the need for investigation of the phenomenon for larger values of the parameter a. However, when the ratio a/δ is of order one or much larger than one, the steady currents can be determined only by the numerical approach briefly sketched in § 4.

When the ratio a/δ is increased to assume large values, the right-hand side of (4.20) tends to become much larger than the left-hand side. However, viscous effects are still significant close to the bottom, where a boundary layer appears to allow the forcing of (4.29)–(4.30).

The unknown order of magnitude of the thickness of the bottom boundary layer $(\delta/a)^{\alpha}$ (in which α is a value to be determined) and the leading-order contributions in the vorticity equation can be found as follows. First of all, the boundary condition (4.29) shows that $\bar{\psi}_1 \sim O[(\delta/a)^{\alpha}]$, while definition (4.24) of the vorticity leads to $\bar{\Omega}_1 \sim O[(\delta/a)^{-\alpha}]$. Moreover, it can be easily verified that $\bar{u}_1 \sim O(1)$ and $\bar{v}_1 \sim O[(\delta/a)^{\alpha}]$. Using these estimates, equation (4.25) shows that α should be equal to 1 to make viscous effects as large as convective ones and, therefore, the thickness of the bottom boundary layer is $O[(\delta/a)]$.

This qualitative prediction is supported by the numerical results shown in figure 6, where the cross-shore velocity component $\bar{u}_1$ is plotted versus Y at $X = 2$ for

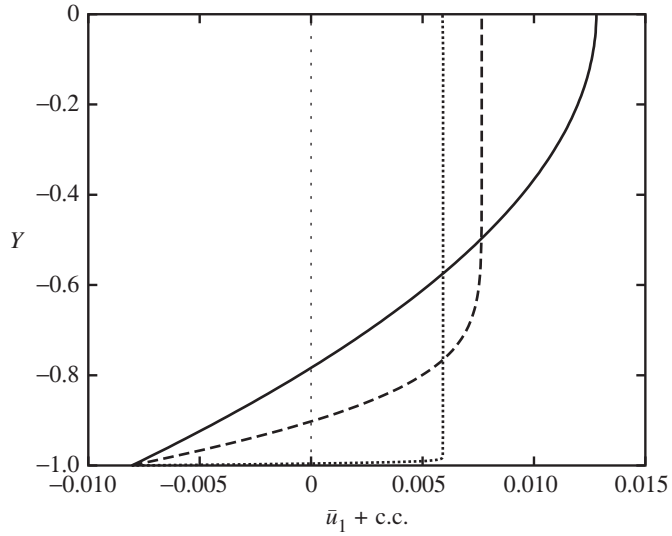

Figure 6. Influence of a/δ on the profiles of the cross-shore velocity for a fully absorbed wave: solid line, $a/\delta \simeq 2.5$; dashed line, $a/\delta \simeq 25$; and dotted line, $a/\delta \simeq 250$. Computational parameters: $X = 2$, $\beta_0 \simeq 0.16$ and $\delta \simeq 0.008$.

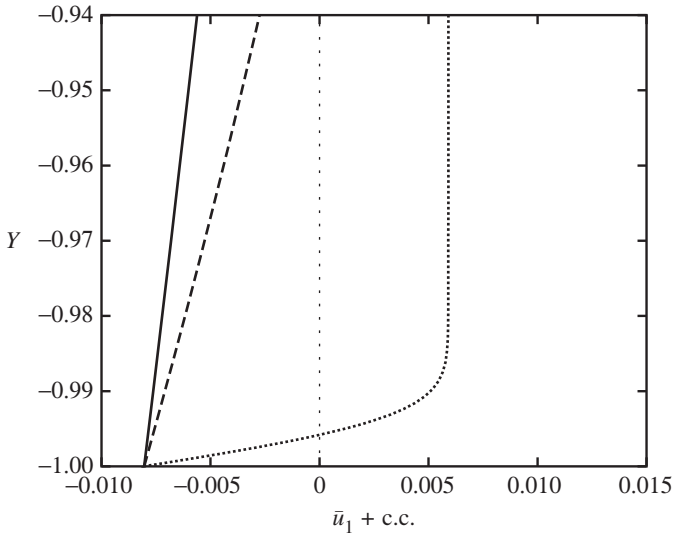

Figure 7. Influence of a/δ on the profiles of the cross-shore velocity for a fully absorbed wave: solid line, $a/\delta \simeq 2.5$; dashed line, $a/\delta \simeq 25$; and dotted line, $a/\delta \simeq 250$. Enlargement of figure 6 near the bottom.

$\beta_0 \simeq 0.16$ and for $a/\delta \simeq 2.5$, 25, 250, respectively. Indeed for the largest value of the ratio a/δ, the velocity profile is almost flat, except close to the wall where a large gradient is present (see figure 7).

On the other hand, for $a/\delta \simeq 2.5$ the velocity profile is close to a parabolic distribution. Since the values of β_0 and δ considered in figures 6 and 7 are equal to those of figure 5, for an incoming wave characterized by a period of 2 s, β and h_0^* are 0.05

Table 1. *Experimental conditions as for Hwung & Lin (1990)*

test number	wave period (s)	wave steepness in deep water (height/length)
1	1.41	0.0186
2	1.23	0.0313
3	0.96	0.0405
4	0.96	0.0617

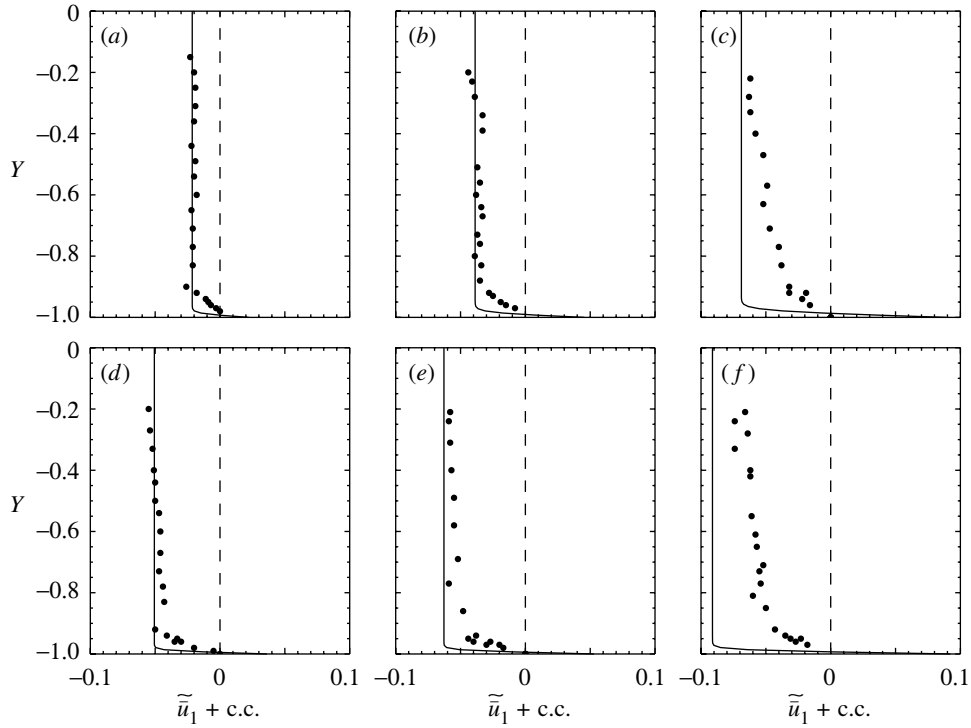

Figure 8. Mass-transport profiles. (*a*)–(*c*) Test 1 and (*d*)–(*f*) test 4. (*a*) $h^* = 174$ mm; (*b*) $h^* = 130$ mm; (*c*) $h^* = 98$ mm; (*d*) $h^* = 174$ mm; (*e*) $h^* = 157$ mm; (*f*) $h^* = 130$ mm. Solid circles represent experimental data, while the solid line represents the solution of (4.24), (4.25) and (4.16). The theoretical results have been obtained for the following values of the parameters. Test 1: $\beta_0 = 0.150$, $\delta = 6.8 \times 10^{-3}$, $a = 1.68$. Test 4: $\beta_0 = 0.102$, $\delta = 5.6 \times 10^{-3}$, $a = 3.15$.

and 0.10 m, respectively. Moreover, the wave amplitude turns out to be 5×10^{-4} m, 5×10^{-3} m and 5×10^{-2} m for a/δ equal to 2.5, 25 and 250, respectively. In particular, the last value of a/δ turns out to be realistic for waves generated in a laboratory wave tank.

Before discussing further results, it is worth pointing out that the theoretical findings have been successfully compared with some recent laboratory data obtained by Hwung & Lin (1990). There are many other sets of data on the steady-velocity components generated by a sea wave propagating over a sloping beach. However, such

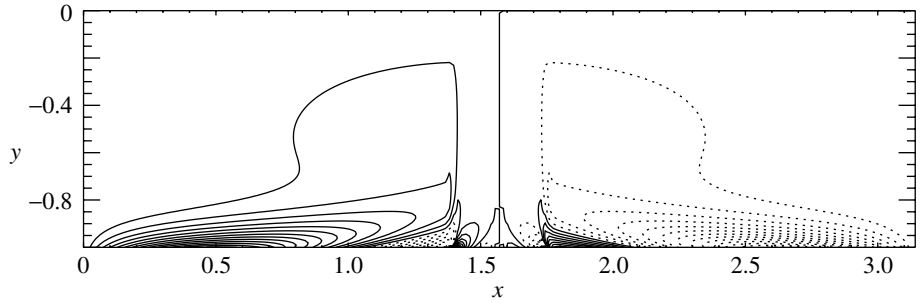

Figure 9. Contours of steady vorticity for a standing wave ($\delta^*/a^* = 0.14$, $\beta_0 = 0$ and $\delta \simeq 0.008$). Solid lines are used to represent positive values, while dotted lines pertain to negative values (contour increase of 5).

data have been mainly obtained inside the surf region or close to the breaker line. Hwung & Lin (1990) measured the mass-transport profiles outside the surf region on a constant sloping beach of slope 1:15, for four monochromatic waves of different characteristics, which led to both plunging (tests 1–3) and spilling (test 4) breaking. Table 1 summarizes the experimental conditions.

In figure 8 the data measured during tests 1 and 4 are shown at different cross-shore sections along with the theoretical predictions. Notice that we adopted a definition of the x-axis (pointing seaward) which differs from that adopted by Hwung & Lin (1990) (shoreward-pointing $\tilde{x}$-axis). Hence, in order to compare the two sets of data we just changed the sign of the model results (i.e. $\tilde{x} = -x$ and $\tilde{\bar{u}}_1 = -\bar{u}_1$).

It is worth pointing out that wave breaking occurred approximately at a water depth h^* equal to *ca.* 8.5 cm for test 1 and *ca.* 11.0 cm for test 4. From figure 8, it appears that the model represents well the mass transport independent of the type of breaking (plunging or spilling) undergone by the incident wave. Some discrepancy, however, can be observed when considering the data relative to the most inshore gauges. Indeed a somehow different behaviour characterizes the experimental data with respect to the theoretical ones. The latter present a very uniform distribution over the vertical, while the former are characterized by a gradually increasing velocity profile from the bottom up to the still-water level. We argue that this is caused by the strong mixing induced by the presence of turbulence which is produced by wave breaking and convected seaward of the breaker line by the steady streaming. This being the case, the performance of the model should not surprise us. Indeed in the analysis the flow is assumed to be turbulence free.

It could be concluded that the analysis provides a good description of the mass transport if a region offshore of the surf zone but not too close to the breaker line is considered.

Present predictions have also been compared with the results described in Iskandarani & Liu (1991*a*), who analysed the steady currents generated by a partly reflected wave propagating over waters of constant depth. For β_0 tending to zero the free-surface displacement (3.11) turns out to be described by a sinusoidal function of x with an amplitude proportional to $\sqrt{\beta_0}$.

However, for a horizontal bed, it is more appropriate to introduce a new definition $\tilde{a}^*$ of the quantity a^* simply equal to the amplitude of the incoming wave at $x^* = 0$. With this new definition and the introduction of the parameter $\tilde{a} = \tilde{a}^*/h_0^*$ (which

substitutes a into (3.1) and (4.17)), the function $\hat{\eta}_{00}$ is a sinusoidal function of x and t with an amplitude which depends on the reflection coefficient $\hat{K}$ but turns out to be of order one. Then equations (4.24) and (4.25) can be solved to determine $\bar{\Omega}_1$.

In figure 9 the vorticity $\bar{\Omega}_1$ is plotted for a fully reflected wave and for $\delta^*/\tilde{a}^* = 0.14$, which is the value considered by Iskandarani & Liu (1991*a*) in their fig. 3*d* (notice the different definitions of the viscous length δ^*). The agreement between present predictions and the results plotted in fig. 3*d* of Iskandarani & Liu's (1991*a*) paper is fair, even though differences can be detected. These differences are present because the results of Iskandarani & Liu (1991*a*) were obtained for a value of the ratio between the water depth h_0^* and the wavelength $\tilde{L}^*$ equal to 0.16, a value too large to be described by the shallow-water approximation. Since all the results described by Iskandarani & Liu (1991*a*) are for $h_0^*/\tilde{L}^*$ equal to 0.16, a detailed quantitative comparison is not possible.

The predictions of the steady-velocity component for different values of the parameters are presented below. To summarize the results, plots of the stream function $\bar{\psi}_1$ in the (x, y)-plane are provided.

In figure 10 the behaviour of $\bar{\psi}_1$ is given for an incoming wave fully absorbed at the coastline, $\beta_0 \simeq 0.16$, $\delta \simeq 0.008$ and for different values of a/δ ($a/\delta = 2.5$, 25, 250).

For the lowest value of the ratio a/δ (see figure 10*a*), the steady flow induced by wave propagation is characterized by a seaward current which has its maximum strength close to the free surface and then decreases while moving towards the sea bed. At about two thirds of the water depth, the steady streaming reverses its direction and the velocity is shoreward directed. Of course, as shown by (5.3), the depth-averaged value of $\bar{u}_1$ is positive and directed towards the deep-water region to compensate for the onshore mass transport induced by the wave in the region between the troughs and the crests. The velocity distribution is similar at different cross-shore locations: when different values of x are considered the strength of the steady currents simply decreases or increases depending on the local water depth. When a larger value of a/δ is considered (see figure 10*b*), the thickness of the water column in which the steady streaming is onshore directed decreases and tends to become infinitesimal if a/δ tends to infinity. Indeed figure 10*c* shows a distribution of $\bar{\psi}_1$ such that $\bar{u}_1$ is positive over practically the whole water depth. Moreover, large values of a/δ lead to a flat velocity distribution, i.e. $\bar{u}_1$ turns out to be almost constant, except close to the bottom in the so-called 'Stuart layer'. In figure 11, the ratio between the convective term in the vorticity equation (4.20) and the term arising from the interaction of the first-order wavefield with itself and with the steady vorticity (i.e. contributions in square brackets in (4.20)) is shown for values of the parameters equal to those of figure 10. It can be easily appreciated that the two terms are of the same order of magnitude in all cases and over the whole water depth, thus indicating the crucial role of the latter contribution in determining the results here described.

Figure 12 shows the patterns of $\bar{\psi}_1$ for the same values of β_0 and δ as in figure 10 and different values of a/δ but for a wave fully reflected at the coastline, $[\hat{K} = (1, 0)]$. When $|\hat{K}|$ is equal to one, the steady flow is characterized by recirculation cells the size and form of which depend on the parameters of the problem. The steady streaming is usually upward directed under the antinodes of the free-surface oscillations, while it is downward directed under the nodes (figure 12*b* shows the loca-

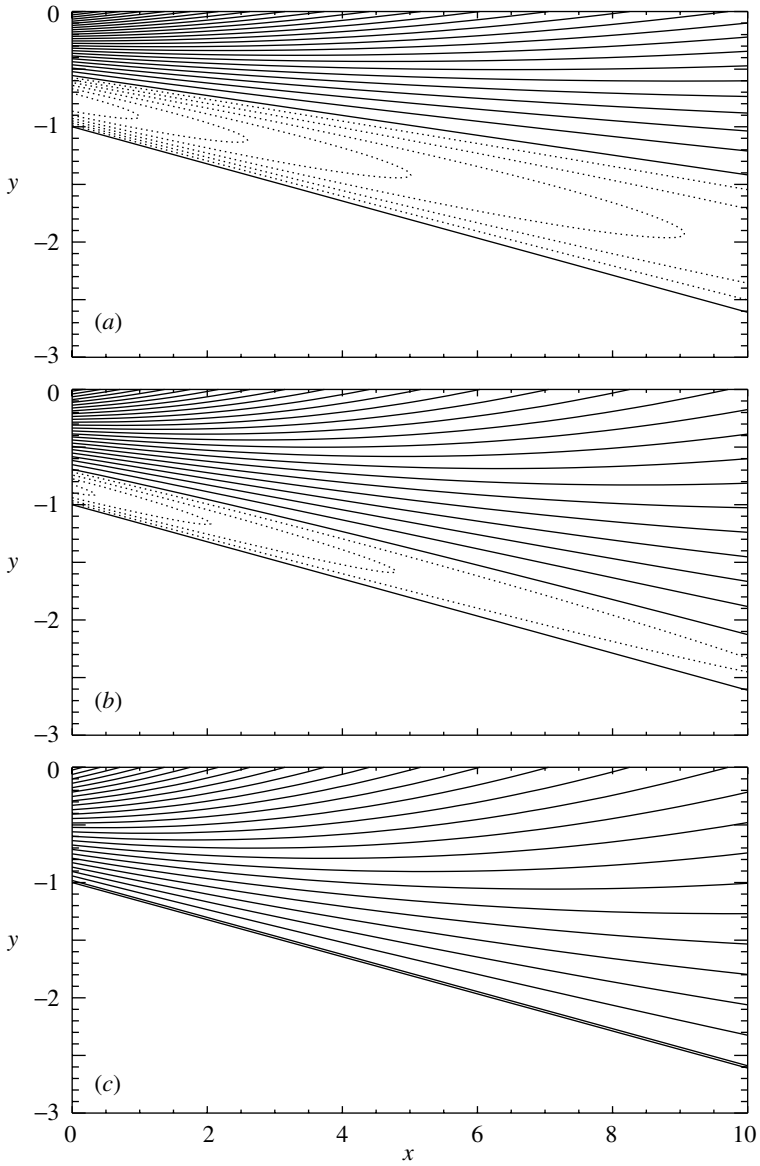

Figure 10. Influence of a/δ on the patterns of the stream function $\bar{\psi}_1$ for a fully absorbed wave at the coastline and for $\beta_0 \simeq 0.16$ and $\delta \simeq 0.008$. Values of a/δ increase from 2.5 (a) to 25 (b) to 250 (c). Solid lines are used to represent positive values (contour increase of 0.0010), while dotted lines pertain to negative values (contour increase of 0.0005).

tions of both nodes and antinodes). For low values of a/δ, vorticity is spread over the whole water column and four recirculating cells per wavelength are generated (see figure 12a).

When increasing values of a/δ are considered, vorticity tends to be stronger close to the bottom and at cross-shore locations where there is an upward-pointing jet of fluid. Here, vorticity, which is generated at the sea bed, is convected towards the free

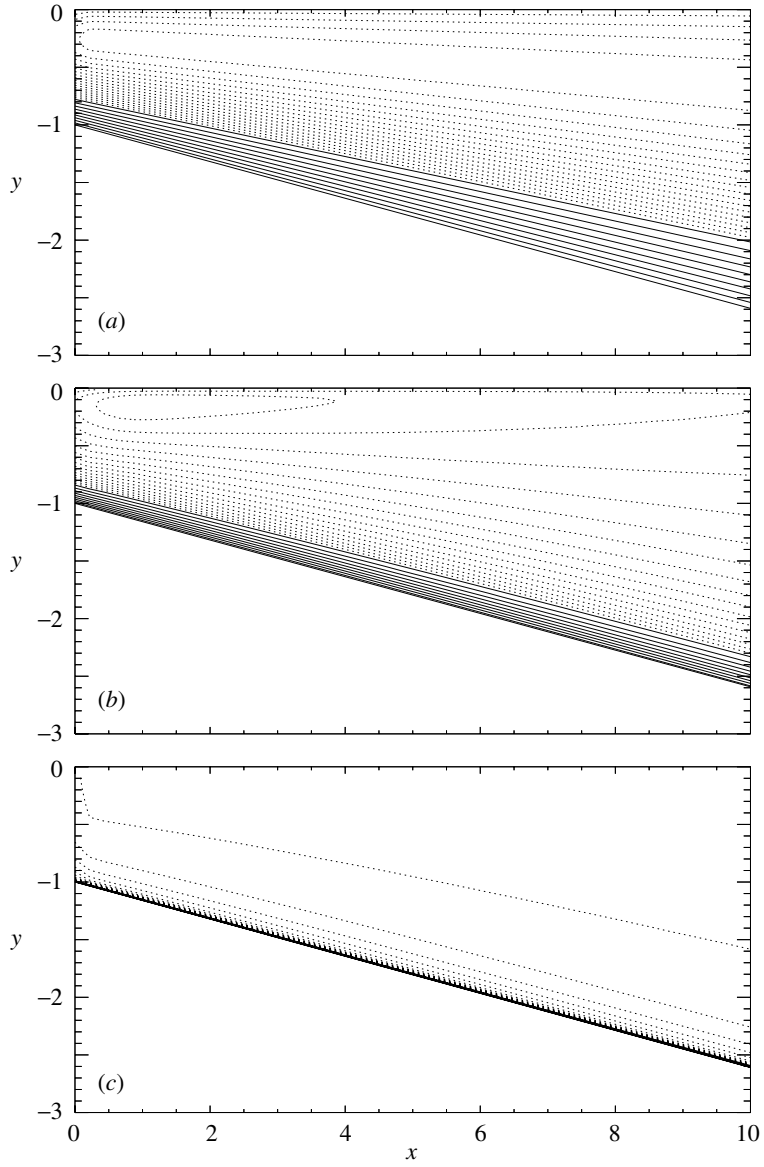

Figure 11. Influence of the term due to the interaction of the first-order wavefield with itself and with the steady vorticity (i.e. contributions in square brackets in (4.20)). Contours represent the ratio between convection and such an interaction term. The parameters are those reported in the caption of figure 10. Solid lines are used to represent positive values (contour increase of 0.15), while dotted lines pertain to negative values (contour increase of 0.075).

surface by the vertical motion of the fluid (see figure 12*c*). Further increases in the ratio a/δ lead to the formation of a second boundary layer, adjacent to the bottom boundary layer (Stokes layer), as for the case of a fully absorbed wave (see figures 6, 7 and 12). However, for a reflected wave, the solution, when a/δ becomes large, is no longer valid because this second boundary layer leaves the bottom and is convected

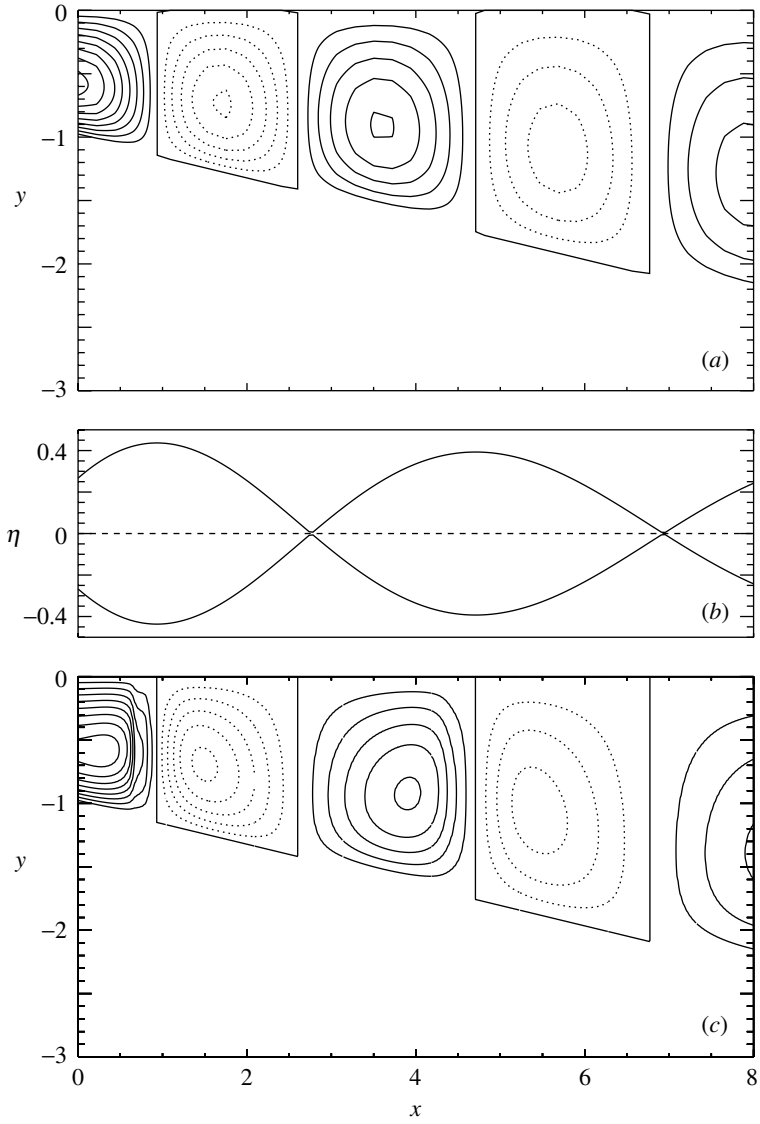

Figure 12. Influence of a/δ on the patterns of the stream function $\bar{\psi}_1$ for a fully reflected wave at the coastline and for $\beta_0 \simeq 0.16$ and $\delta \simeq 0.008$. Values of a/δ increase from 2.5 (a) to 12.7 (c). Solid lines are used to represent positive values, while dotted lines pertain to negative values (contour increase of 0.002). (b) The range of oscillations of the free surface (scaled with a^*).

in the vertical direction, generating large horizontal gradients of velocity and causing the failure of the shallow-water approximation.

The presence of vorticity convection in the vertical direction is more evident in figure 13, which is an enlargement of figure 12c. Indeed at $x \simeq 0.6$ the streamlines gather, showing the presence of strong vertical velocities. At this cross-shore location the vorticity, which is generated at the bottom, leaves the sea bed, tending to form shear layers.

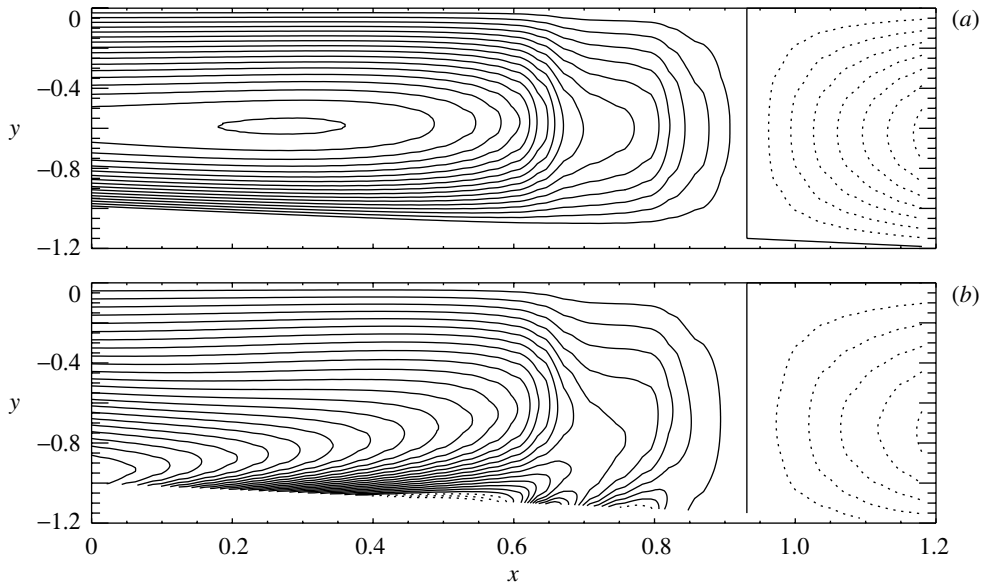

Figure 13. Upward convection of vorticity for a fully reflected wave at the coastline ($a/\delta = 12.7$, $\beta_0 \simeq 0.16$ and $\delta \simeq 0.008$). (*a*) Stream function $\bar{\psi}_1$ (contour increase of 0.001). (*b*) Vorticity $\bar{\Omega}_1$ (contour increase of 0.01). Solid lines are used to represent positive values, while dashed lines pertain to negative values.

It is worth pointing out that a change of the phase of the reflection coefficient leads to a shoreward or offshore shift of the recirculating cells and, in particular, the stream function vanishes at $x = 0$ if the phase of $\hat{K}$ is chosen in such a way that $\hat{u}_{00}$ vanishes at such cross-shore locations.

Until now, results have been presented relative to the extreme cases of both a fully reflected wave and a wave which breaks at the coast with a complete dissipation of its energy. Examples of the stream function $\bar{\psi}_1$ for partly reflected waves are given in figure 14 for realistic values of the reflection coefficient $|\hat{K}|$ and fixed values β_0, δ and a/δ. The fluid domain can be split into two layers. In the upper one, an offshore-directed current is present which is more intense close to the free surface and becomes weaker moving towards the bottom. In the lower layer, recirculating cells are generated. The strength of these cells decreases moving in the offshore direction and in figure 14 only the three cells closest to the beach appear.

We believe that the results obtained for the extreme conditions of fully absorbed and reflected waves along with those shown in figure 14 are adequate to illustrate all the features of the phenomenon and, for the sake of brevity, we have not reported on results concerning different values of $\hat{K}$ here.

6. Conclusions

In §§ 3 and 4 we have determined the flow induced by a sea wave propagating on a gently sloping bottom and partly reflected at the coastline, focusing our attention in the region offshore of the breaker line. To solve the problem the water depth has been assumed to be much smaller than the length of the incoming wave and its amplitude has been assumed to be much smaller than the local depth. Moreover,

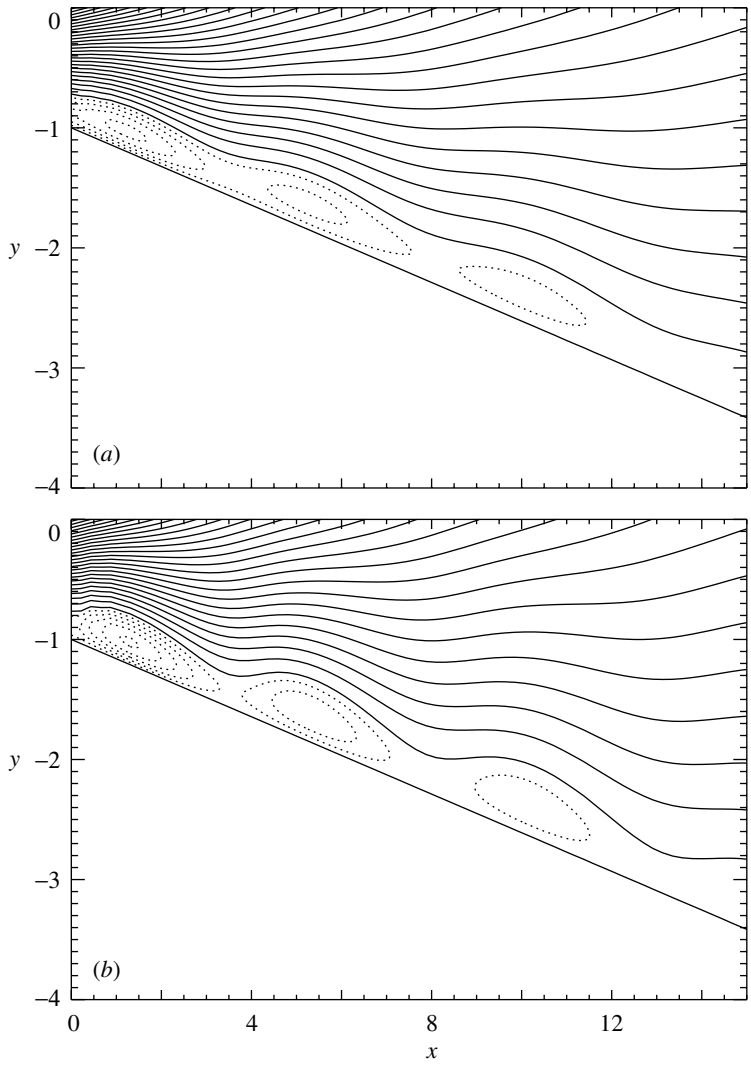

Figure 14. Influence of a/δ on the patterns of the stream function $\bar{\psi}_1$ for a partly reflected wave at the coastline and for $\beta_0 \simeq 0.16$, $\delta \simeq 0.008$ and $a/\delta = 25$. Values of $|K|$ increase from 0.1 (a) to 0.2 (b). Solid lines are used to represent positive values (contour increase of 0.0010), while dotted lines pertain to negative values (contour increase of 0.0005).

the flow Reynolds number is supposed to be large enough to assume that viscous effects in the momentum equation are confined within a bottom boundary layer. The major outcome of the analysis is the determination of the steady currents induced by nonlinear effects both in the bottom boundary layer and in the whole water column up to the free surface.

The differences between the present results and those describing the undertow structure in the surf region are due to the different physical balances which take place inside and outside the surf zone. Seaward of the breaker line there is a balance between the gradient of the mean water level and the term due to the nonlinear self-interaction of the horizontal orbital velocity (see equation (4.5)). Indeed the

shear-stress term is negligible both when the flow is dominated by viscous effects (as presently assumed) and when the weak turbulence, which is possibly present seaward of the breaker line, is taken into account. Under these circumstances the steady-velocity field cannot be derived directly from (4.5) and information on the vorticity distribution is needed. On the other hand, in the surf region, the presence of the strong turbulence induced by wave breaking makes the shear stress term as large as the other terms and the undertow structure can be derived directly from the momentum equation, once an appropriate turbulence closure model is adopted, with no need to study the vorticity distribution.

In order to apply the present analysis to field conditions, improvements are necessary. First, the study of the flow in the bottom boundary layer should be modified since the flow regime here is often turbulent. Moreover, the presence of weak turbulence should also be considered far from the bottom where it increases any mixing processes and, in particular, the diffusion of vorticity. Finally, it would be worthwhile to investigate arbitrary bottom configurations. A first attempt to take into account the presence of turbulence has been performed by Blondeaux *et al*. (1999), even though a more refined turbulence model should be used to obtain more accurate results.

Support from the Office of Naval Research through the NICOP grant N00014-97-1-0790, from the European Union through the contract MAS3-CT97-0115 (SEDMOC) and from the Ministero dell'Università e della Ricerca Scientifica e Tecnologica (MURST) and the University of Genova under the contract COFIN'97 'Morfodinamica Fluviale e Costiera' is gratefully acknowledged. The authors thank Professor E. Thornton for stimulating them to tackle the problem and for interesting discussions on some aspects of the phenomenon.

References

Abramowitz, M. & Stegun, I. A. 1964 *Handbook of mathematical functions*. New York: Dover.

Blondeaux, P. 1990 Sand ripples under sea waves. Part 1. Ripple formation. *J. Fluid Mech.* **218**, 1–17.

Blondeaux, P., Stanton, T., Thornton, E. & Vittori, G. 1999 Modelling cross-shore mass transport under sea waves. In *Proc. IAHR-RCEM Symp.*, vol. 1, pp. 445–454.

Carter, T. G., Liu, P. F.-L. & Mei, C. C. 1973 Mass transport by waves and offshore sand bedforms. *J. Wtrwys Harb. Div. ASCE* **99**, 165–184.

Cox, D. T., Kobayashi, N. & Okayasu, A. 1995 Experimental and numerical modeling of surf zone hydrodynamics. Report No. CACR-95–07, Center for Applied Coastal Research, University of Delaware, Newark, DE.

Craik, A. D. D. 1982 The drift velocity of water waves. *J. Fluid Mech.* **116**, 187–205.

Dally, W. B. & Dean, R. G. 1984 Suspended sediment transport and beach evolution. *J. Wtrwy Port Coast. Ocean Engng* **110**, 15–33.

Deigaard, R., Justesen, P. & Fredsøe, J. 1991 Modeling of undertow by a one-equation turbulence model. *Coastal Engng* **15**, 431–458.

Dore, B. D. 1976 Double boundary layers in standing surface waves. *Pure Appl. Geophys.* **114**, 629–637.

Fredsøe, J. & Deigaard, R. 1992 *Mechanics of coastal sediment transport*. World Scientific.

Friedricks, K. O. 1948 Water waves on a shallow sloping beach. *Commun. Pure Appl. Math.* **1**, 109–134.

Fromm, J. E. 1963 A method for computing non-steady incompressible viscous fluid flows. Los Alamos Scientific Laboratory, Report No. LA-2910, Los Alamos, NM.

Gresho, P. M. & Sani, R. L. 1990 Introducing four benchmark solutions. *Int. J. Numer. Meth. Fluids* **11**, 951–952.

Haddon, E. W. & Riley, N. 1983 A note on the mean circulation in standing waves. *Wave Motion* **5**, 43–48.

Hara, T. & Mei, C. C. 1989 Oscillating flows over periodic ripples. *J. Fluid Mech.* **211**, 183–209.

Harlow, F. H. & Fromm, J. E. 1964 Dynamics and heat transfer in the Von Karman wake of a rectangular cylinder. *Phys. Fluids* **7**, 1147–1156.

Hunt, J. N. & Johns, B. 1963 Currents induced by tides and gravity waves. *Tellus* **15**, 343–351.

Hwung, H. H. & Lin, C. 1990 The mass transport of waves propagating on a sloping bottom. In *Proc. 22nd Int. Conf. Coastal Engineering, ASCE*, pp. 544–556. Reston, VA: ASCE.

Iskandarani, M. & Liu, P. L.-F. 1991*a* Mass transport in two-dimensional water waves. *J. Fluid Mech.* **231**, 395–415.

Iskandarani, M. & Liu, P. L.-F. 1991*b* Mass transport in three-dimensional water waves. *J. Fluid Mech.* **231**, 417–437.

Katsanis, T. 1967 A computer program for calculating velocities and streamlines for two-dimensional incompressible flow in axial blade rows. NASA Report TN D-3762.

Komar, P. D. 1998 *Beach processes and sedimentation*. Englewood Cliffs, NJ: Prentice-Hall.

Lau, J. & Travis, B. 1973 Slowly varying Stokes waves and submarine longshore bars. *J. Geophys. Res. Oceans* **78**, 4489–4497.

Li, L. & Dalrymple, R. A. 1998 Instabilities of the undertow. *J. Fluid Mech.* **369**, 175–190.

Liu, P. F.-L. 1977 Mass transport in water waves propagated over a permeable bed. *Coastal Engng* **1**, 79–96.

Longuet-Higgins, M. S. 1953 Mass transport in water waves. *Phil. Trans. R. Soc. Lond.* A **245**, 535–581.

Lyne, W. H. 1971 Unsteady viscous flow over a wavy wall. *J. Fluid Mech.* **50**, 33–48.

Matsunaga, N., Takehara, K. & Awaya, Y. 1988 Coherent eddies induced by breakers on a sloping bed. In *Proc. 21st Int. Conf. Coastal Engineering, ASCE*, pp. 234–245. Reston, VA: ASCE.

Matsunaga, N., Takehara, K. & Awaya, Y. 1994 The offshore vortex train. *J. Fluid Mech.* **276**, 113–124.

Mei, C. C. 1989 *The applied dynamics of ocean surface waves*. World Scientific.

Peregrine, D. H. 1967 Long waves on a beach. *J. Fluid Mech.* **27**, 815–827.

Phillips, O. M. 1977 *Dynamics of the upper ocean*. Cambridge University Press.

Riley, N. 1984 Progressive surface waves on a liquid of non-uniform depth. *Wave Motion* **6**, 15–22.

Riley, N. 2001 Steady streaming. *A. Rev. Fluid Mech.* **33**, 43–65.

Roache, P. J. 1972 *Computational fluid dynamics*. Albuquerque, NM: Hermosa.

Sleath, J. F. A. 1976 On rolling grain ripples. *J. Hydraul. Res.* **14**, 69–81.

Stive, M. J. F. & De Vriend, H. J. 1994 Shear stress and mean flow in shoaling and breaking waves. In *Proc. 24th Conf. Coastal Engineering, ASCE*, 594–608. Reston, VA: ASCE.

Stive, M. J. F. & Wind, H. G. 1986 Cross-shore mean flow in the surf zone. *Coastal Engng* **10**, 325–340.

Stoker, J. J. 1957 *Water waves*. Wiley Interscience.

Stokes, G. G. 1847 On the theory of oscillatory waves. *Trans. Camb. Phil. Soc.* **8**, 441–455.

Stuart, J. T. 1966 Double boundary layer in oscillatory viscous flows. *J. Fluid Mech.* **24**, 637–687.

Svendsen, I. A. 1984 Mass flux and undertow in a surf zone. *Coastal Engng* **8**, 247–365.

Svendsen, I. A., Schaffer, H. A. & Hansen, J. B. 1987 The interaction between the undertow and the boundary-layer flow on a beach. *J. Geophys. Res. Oceans* **92**, 11 845–11 856.

Thom, A. 1928 An investigation of fluid flow in two-dimensions. Aerospace Research Center, R. and M., No. 1194, UK.

Thoman, D. C. & Szewczyk, A. A. 1966 Numerical solution of time dependent two dimensional flow of viscous, incompressible fluid over stationary and rotating cylinders. Technical Report 66-14, Heat Transfer and Fluid Mechanics laboratory, Department of Mechanical Engineering, University of Notre Dame, Notre Dame, IN.

Van Rijn, L. C. 1990 Sediment transport in combined waves and currents. In *Proc. Euromech 262: Sand transport in Rivers, Estuaries and the Sea* (ed. R. Soulsby & R. Bettes), pp. 3–15. Rotterdam: Balkema.

Van Rijn, L. C. 1993 *Principles of sediment transport in rivers, estuaries and coastal seas.* Amsterdam: Aqua Publications.

Vittori, G. 1989 Nonlinear viscous oscillatory flow over a small amplitude wavy wall. *J. Hydraul. Res.* **27**, 267–280.

Vittori, G. & Blondeaux, P. 1996 Mass transport under sea waves propagating over a rippled bed. *J. Fluid Mech.* **314**, 247–265.

Wen, J. & Liu, P. L.-F. 1994 Mass transport under partially reflected waves in a rectangular channel. *J. Fluid Mech.* **266**, 121–145.

Yu, J. & Mei, C. C. 2000 Formation of sand bars under surface waves. *J. Fluid Mech.* **416**, 315–348.

As this paper exceeds the maximum length normally permitted,
the authors have agreed to contribute to production costs.